

REVERBERATION MAPPING AND THE PHYSICS OF ACTIVE GALACTIC NUCLEI

HAGAI NETZER

*School of Physics and Astronomy and The Wise Observatory,
Tel Aviv University, Tel Aviv 69978, ISRAEL*

AND

BRADLEY M. PETERSON

*Department of Astronomy, The Ohio State University, 174
West 18th Avenue, Columbus, OH 43210, USA*

Abstract. Reverberation-mapping campaigns have revolutionized our understanding of AGN. They have allowed the direct determination of the broad-line region size, enabled mapping of the gas distribution around the central black hole, and are starting to resolve the continuum source structure. This review describes the recent and successful campaigns of the International AGN Watch consortium, outlines the theoretical background of reverberation mapping and the calculation of transfer functions, and addresses the fundamental difficulties of such experiments. It shows that such large-scale experiments have resulted in a “new BLR” which is considerably different from the one we knew just ten years ago. We discuss in some detail the more important new results, including the luminosity–size–mass relationship for AGN, and suggest ways to proceed in the near future.

1. Introduction

Continuum variability was one of the earliest recognized characteristics of quasars, the highest-luminosity active galactic nuclei (AGN). In contrast, continuum variations were not confirmed in their lower-luminosity cousins, Seyfert galaxies, until a quarter century after they had been identified as a separate class of object. Ultimately the shared characteristic of continuum variability helped establish the link between quasars and Seyfert galaxies, and in both classes of object it led immediately to recognition that large-

amplitude, short time-scale variations place strong constraints on the size of the continuum-emitting region. This is a cornerstone of the black-hole model of active nuclei. While it has been realized subsequently that the most violent variability seen in AGN arises in a relativistically beamed component (which dominates the spectra of the subset of AGN known as “blazars”), the conclusion that the continuum-emitting region is small is still valid, and indeed the physical scales inferred from variability are consistent with thermal emission from accretion disks. The origin of the variations remains unknown.

Some fifteen years ago was it becoming apparent that the broad emission lines seen in AGN spectra also vary, both in flux and in profile. It was established fairly quickly that the emission-line fluxes vary in response to continuum changes, but the exact time scales for response remained controversial on account of the relatively few, poorly spaced observations that had been obtained in even the best-studied cases. Line-profile variations had been clearly detected in a few cases, and it was suggested by several authors that these might be attributable to “excitation inhomogeneities” resulting from non-uniform illumination of the broad-line region (BLR) due to light travel-time effects. It was widely appreciated that this afforded an opportunity to map out the spatial and kinematic distribution of the line-emitting clouds: by carefully following continuum variations and their subsequent effect on the emission-line fluxes and profiles, one can highly constrain the phase-space distribution of the line-emitting gas. Blandford & McKee (1982) were the first to articulate the mathematical formalism for this process, which they called “reverberation mapping”.

The potential importance of the reverberation-mapping technique to AGN astrophysics is profound: if we can determine the structure and kinematics of the BLR, it is possible to determine the effects of various forces in the immediate vicinity of the central engine (gravity and radiation pressure) and under some conditions, to determine the mass of the central engine itself, thus possibly testing the black-hole paradigm directly. The BLR itself is thought to be comprised of a large number (at least $\sim 10^5$, and by some arguments more than 10^8) of individual clouds that have, by nebular standards, quite high densities ($n_e \gtrsim 10^9 \text{ cm}^{-3}$). These clouds move highly supersonically, at thousands of kilometers per second, and cover only about 10% of the sky as seen from central source. The BLR is much too small to be resolvable spatially, with an angular extent of only $\sim 10 \mu\text{arcsec}$ even in nearby ($cz/H_0 \approx 50 \text{ Mpc}$) Seyfert galaxies.

2. Reverberation-Mapping Techniques

2.1. FUNDAMENTALS

The basic idea of reverberation mapping is similar to that which underlies, for example, Doppler-weather mapping: the time-delayed, Doppler-shifted response of a system to a known input signal is used to infer the structure and kinematics of the responding system. In the case of reverberation mapping, we passively observe the input signal, which is generated by the AGN continuum source. In the absence of reasons to assume otherwise, we make the following simplifying assumptions:

1. The continuum is supposed to originate in a single, central source whose UV/optical radiation producing size is thought to have a spatial extent of 10–100 gravitational radii, $R_g \approx 1.5 \times 10^{13} (M/10^8 M_\odot)$ cm. This estimate is based on accretion-disk models that are generally consistent with the observable parameters. We note in particular that isotropic emission from the central source does not have to be assumed.
2. The light-travel times across the BLR are found to be in the range of days to weeks. The time scale for response of individual BLR clouds to changes in the ionizing flux is given by the recombination time $\tau_{\text{rec}} \approx (n_e \alpha_B)^{-1}$, where α_B is the case B hydrogen recombination coefficient. For BLR densities, $\tau_{\text{rec}} \approx 1$ hr, so the cloud response time is virtually instantaneous and can be neglected. We must also assume that the BLR structure and kinematics are constant over the duration of the monitoring experiment. This places practical time limits on the duration of single experiments, as we discuss further below.
3. There is a simple, although not necessarily linear, relationship between the observed UV or optical continuum and the ionizing continuum that is driving the line variations. In this context, “simple” means that the continuum variations in these different continuum bands appear to be generally similar, without pronounced differences in the relative structure of the light curves.

The duration of a monitoring campaign $\tau(\text{campaign})$ is never optimal because of the very nature of the gas distribution and velocity field of the BLR. As emphasized below, one of the most important new results of the AGN Watch campaigns is the evidence for a “thick” BLR geometry in several objects. This means that the outer edge of the cloud system is tens, and perhaps hundreds, of light days away from the continuum source, while the inner boundary is only a few light days away. Assuming a BLR which extends from R_{in} to R_{out} , the observed line response reflects continuum variations that occurred at times up to R_{out}/c before the beginning of the observation. The first R_{out}/c days of the campaign thus can be of limited use. On the other hand, the dynamical time of the system at R_{in} determines

the maximum useful monitoring period since the gas distribution is likely to change on this time scale. This time is given by

$$\tau_{\text{dyn}} = xR_{\text{out}}/V_{\text{in}} \quad (1)$$

where V_{in} is the typical velocity at R_{in} , and $x = R_{\text{in}}/R_{\text{out}}$. Using $\beta_{\text{in}} = V_{\text{in}}/c$, we find

$$\tau(\text{campaign}) \approx \frac{R_{\text{out}}}{c} \left(\frac{x}{\beta_{\text{in}}} - 1 \right). \quad (2)$$

Assuming Keplerian orbits, the velocity in the innermost part is obtained from the full width at zero intensity (FWZI) of the emission lines. Typically, this is $\beta_{\text{in}} \approx 0.03$. Since x is of order 0.1 or smaller, the useful campaign time is of the order of $2R_{\text{out}}/c$ or less, i.e., a few months for typical Seyfert 1 luminosities. Obviously, the gas distribution (and the transfer function, see below) may be stable over many dynamical times, but this has not yet been established. Thus, multiple-year campaigns are not necessarily more useful than few-month campaigns in determining the BLR gas distribution and velocity field.

2.2. THE TRANSFER FUNCTION

Under the assumptions outlined above, the emission-line response as a function of time and line-of-sight velocity (i.e., Doppler shift) can be written as

$$L(v, t) = \int_{-\infty}^{\infty} \Psi(v, \tau) C(t - \tau) d\tau, \quad (3)$$

where $C(t)$ is the continuum light curve, and $\Psi(v, \tau)$ is the “transfer function” which depends on the BLR geometry, kinematics, and reprocessing physics. The goal of reverberation-mapping experiments is to provide light curves $C(t)$ and $L(v, t)$ that can be used to solve for the transfer function, and infer the characteristic of the emission-line cloud system. A stable and unique solution to an integral equation of this form requires a large amount of high-quality data, and this is the practical difficulty in reverberation mapping. In practice, high-quality spectra of faint objects are not easy to come by, and as a result most experiments to date have focused on the somewhat simpler problem of solving for the *one-dimensional transfer function* $\Psi(\tau)$, which gives the response of the entire emission line integrated over line-of-sight velocity, i.e.,

$$L(t) = \int_{-\infty}^{\infty} \Psi(\tau) C(t - \tau) d\tau. \quad (4)$$

Even more often, the actual data are so sparse that all we can determine is the first moment of $\Psi(\tau)$; it is easily shown (Penston 1991; Peterson 1993)

that convolving eq. (4) with $C(t)$ yields

$$\text{CCF}(\tau) = \int \Psi(\tau') \text{ACF}(\tau - \tau') d\tau', \quad (5)$$

where $\text{CCF}(t)$ and $\text{ACF}(t)$ are the line–continuum cross-correlation function and continuum autocorrelation function, respectively. Cross-correlation of $C(t)$ and $L(t)$ thus yields a first moment of $\Psi(\tau)$, a time scale for emission-line response that is often referred to as the emission-line “lag”.

Equations (3) and (4) are *linear* equations, which seems to introduce another hidden assumption that is contrary to our previous statement that linearity does not need to be assumed for the line response. However, in practice, the transfer equation is solved by replacing $L(t)$ and $C(t)$ with their difference from the mean values, e.g., $\Delta L(t) = L(t) - \langle L \rangle$, which removes the effects of non-variable components and is equivalent to a first-order expansion of the transfer equation. Thus, mild nonlinearity does not pose a problem.

2.3. AN EXAMPLE

The transfer function introduced earlier gives the observed response of an emission line as a function of time delay and line-of-sight velocity to a delta-function continuum outburst, as is obvious from eq. (3). For illustrative purposes, we will consider the response of a simple and specific, but easily generalizable and even possibly relevant, BLR model, namely clouds on randomly inclined, circular Keplerian orbits. Consider first clouds in orbits at inclination $i = 90^\circ$, i.e., with the line of sight in the orbital plane. Positions along the orbital path are specified by the polar coordinates r and θ as defined in Fig. 1a. Each position on the orbit projects to a unique position in velocity–time–delay space, as shown in Fig. 1b. An isotropically emitted continuum outburst will be followed by an emission-line response that is time delayed by the additional path length to the observer that must be traversed by (a) the ionizing photons that travel outward from the central source and are intercepted by BLR clouds and (b) the resulting emission-line photons that are emitted in the direction of the observer; such a time-delayed path is shown as a dotted line in Fig. 1a. At some time delay τ , the emission-line response recorded by the observer will be due to all clouds that lie on a surface of constant time delay (an “isodelay surface”) given by the length of the dotted path in Fig. 1a,

$$\tau = (1 + \cos \theta)r/c, \quad (6)$$

which is the equation of a parabola in polar coordinates. The intersection of the isodelay surface and the cloud orbit identifies the clouds that are re-

sponding at time delay τ . If both clouds shown in Fig. 1a are moving counterclockwise at orbital speed $V_{\text{orb}} = (GM/r)^{1/2}$, where M is the mass of the central source, their observed Doppler-shifted velocities are $v = \pm V_{\text{orb}} \sin \theta$, and thus the locations of the two clouds project to the two different points in velocity–time–delay space, as shown in Fig. 1b. The entire circular orbit is seen to project to an ellipse in the velocity–time–delay diagram; the zero time–delay point represents the BLR clouds that lie along the line of sight (at $\theta = 180^\circ$ and line-of-sight velocity $v = 0$), and the largest line-of-sight velocities are measured at $\theta = \pm 90^\circ$, where $\tau = r/c$. The range of time delays extends up to $2r/c$, corresponding to the response from the far side of the BLR (i.e., $\theta = 0^\circ$). If we consider identical orbits at lower inclinations, it is easy to see that the range of time delays decreases from $[0, 2r/c]$ to $[(1 - \sin i)r/c, (1 + \sin i)r/c]$, and line-of-sight velocities similarly decrease by a factor of $\sin i$. The projection of such an orbit into velocity–time–delay space is thus an ellipse that has the same center (at $v = 0$, $\tau = r/c$) and ellipticity, but axes that are smaller by a factor of $\sin i$. For $i = 0^\circ$, the ellipse contracts to a single point at time delay r/c and line-of-sight velocity $v = 0$. For a system of clouds in circular orbits of radius r and random inclinations, the ellipse shown in Fig. 1b becomes completely filled in, as shown in Fig. 1c, and this is the transfer function for a system of clouds in circular Keplerian orbits of radius r and random inclinations.

How does the transfer function change if the continuum emission is not isotropic? To illustrate, we now consider the case where the continuum radiation is confined to biconical beams of semi-opening angle ω at inclination i_{beam} to the line of sight, as shown in Fig. 2a. On spatially resolved scales, AGN show such biconical structure, although it is not at all obvious that this geometry applies on scales as small as the BLR. A biconical beam illuminates the BLR clouds during only *parts* of their orbits, and as shown in Fig. 2b, emission-line response is observed only in certain loci in the velocity–time–delay plane. Again, extending this to a system of BLR clouds in circular orbits of random inclination, the ellipses in the velocity–time–delay plane become partially filled in, as shown in Fig. 2c. The effects of varying both ω and i_{beam} are shown by Goad & Wanders (1996).

It is straightforward to consider more complex models, especially if the response can be assumed to be approximately linear, in which case transfer functions for complex BLR geometries and continuum anisotropies can be constructed by addition of properly weighted simple transfer functions. For example, partial continuum anisotropy can be modeled as a sum of isotropic and anisotropic geometries. Similarly, the response of a disk can be modeled by a summation of transfer functions for circular Keplerian orbits of various r and fixed i . The transfer function for a thick spherical shell (as in Figs. 1c and 2c) can be constructed by adding together transfer functions for thin

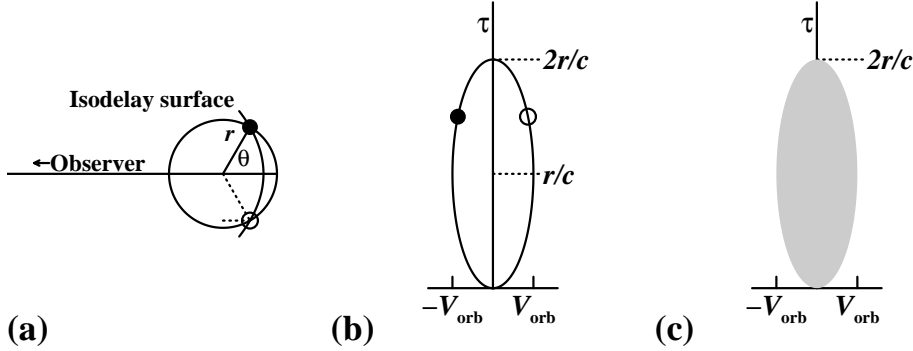


Figure 1. (a) In this illustrative model, the BLR clouds are distributed along a circular orbit centered on the central continuum source at inclination $i = 90^\circ$, with the clouds orbiting counterclockwise. Emission-line clouds respond to a continuum outburst with time delay $\tau = (1 + \cos \theta)r/c$, which compared with the photons from the central source that travel directly to the observer, is the additional path length this signal must travel to the distant observer to the left, as shown by the dotted line. At the time delay shown, two clouds are responding, the upper one approaching the observer and the lower one receding. (b) The points on the circular orbit in (a) project to an ellipse in the velocity–time-delay plane. The locations of the two clouds in (a) are shown. (c) For circular orbits at inclinations less than 90° , the axes of both of the ellipses are decreased by a factor $\sin i$ and the center remains at $v = 0, \tau = r/c$. Thus, for a random distribution of inclinations, the response of the BLR occurs over the full range of radial velocities and time delays limited by the $i = 90^\circ$ case.

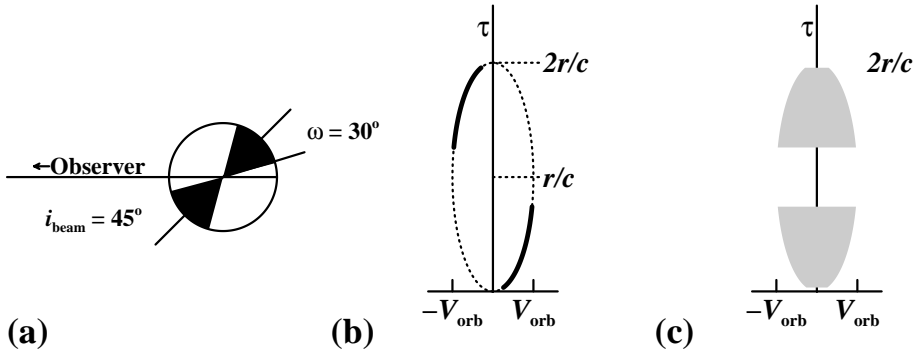


Figure 2. (a) The BLR clouds are distributed along a circle as in Fig. 1, but are now illuminated by an anisotropic continuum (shaded) of opening half-angle $\omega = 30^\circ$ and inclined to the line of sight by $i_{\text{beam}} = 45^\circ$. (b) Since only part of the orbit in (a) is illuminated, only certain loci in the velocity–time-delay plane show emission-line response. (c) For a random distribution of *orbital* inclinations, the response of the BLR is similarly localized in time delay. There is no response in this case (i) near time delay r/c because the continuum does not illuminate any material in orbits with $i \approx 0^\circ$ or (ii) near $\tau = 0$ or $\tau = 2r/c$ since the material along the light of sight is out of the beam.

spherical shells of varying radius; note that as r increases, the velocity–time-delay ellipses become taller and narrower, as the major axis is proportional to r and the minor axis decreases like $r^{-1/2}$.

In Fig. 3, we show as an example a thick-shell model that is an extension of the thin-shell model in Fig. 2, and uses the same continuum beaming parameters. We chose this particular model for two reasons: first, both the one-dimensional transfer function and the variable part of the line profile are double peaked. This makes the important point that such structures are *not* unambiguous signatures of rotating disks or biconical flows (e.g., Welsh & Horne 1991; Pérez, Robinson, & de la Fuente 1992). Second, this particular model seems to be grossly *consistent* with the observed transfer function in one of the best-studied cases, the C IV line in NGC 5548, as we will discuss below.

We close this part of the discussion by reminding the reader that the transfer function does *not* give a model-independent six-dimensional map of the BLR in phase space; the velocity-dependent response of an emission line localizes the gas only to an isodelay surface. The transfer function does, however, provide a strong constraint on the phase-space distribution of the BLR gas, and one must test BLR models by computing transfer functions for various lines and comparing these with the observations. It is also important to remember that the transfer function maps out the *responsivity* of the emission-line gas. We shall come back to this point in §4.

3. Reverberation-Mapping Experiments

Equations (3) and (4) are examples of one of the most common types of problems encountered in physics, a convolution integral with an unknown Green’s function, which we here call the transfer function. The observational goal of reverberation-mapping experiments is to use the light curves $C(t)$ and $L(v, t)$ to solve for the transfer function and then use this to test directly various models of the BLR. What makes the reverberation problem different from other applications is that the sampling of $C(t)$ and $L(v, t)$ is nearly always irregular, limited in both temporal resolution and duration, and the data are often quite noisy and sometimes plagued by systematic errors. These limitations have led to development of specialized methodologies for time-series analysis. The obvious method of Fourier inversion (which was what was originally suggested by Blandford & McKee 1982) performs poorly on account of the limitations listed above. Better methods include the maximum entropy method (MEM; Horne 1994, and this volume), the SOLA method (Pijpers & Wanders 1994), and regularized linear inversion (Krolik & Done 1995). Even cross-correlation techniques (eq. 5)

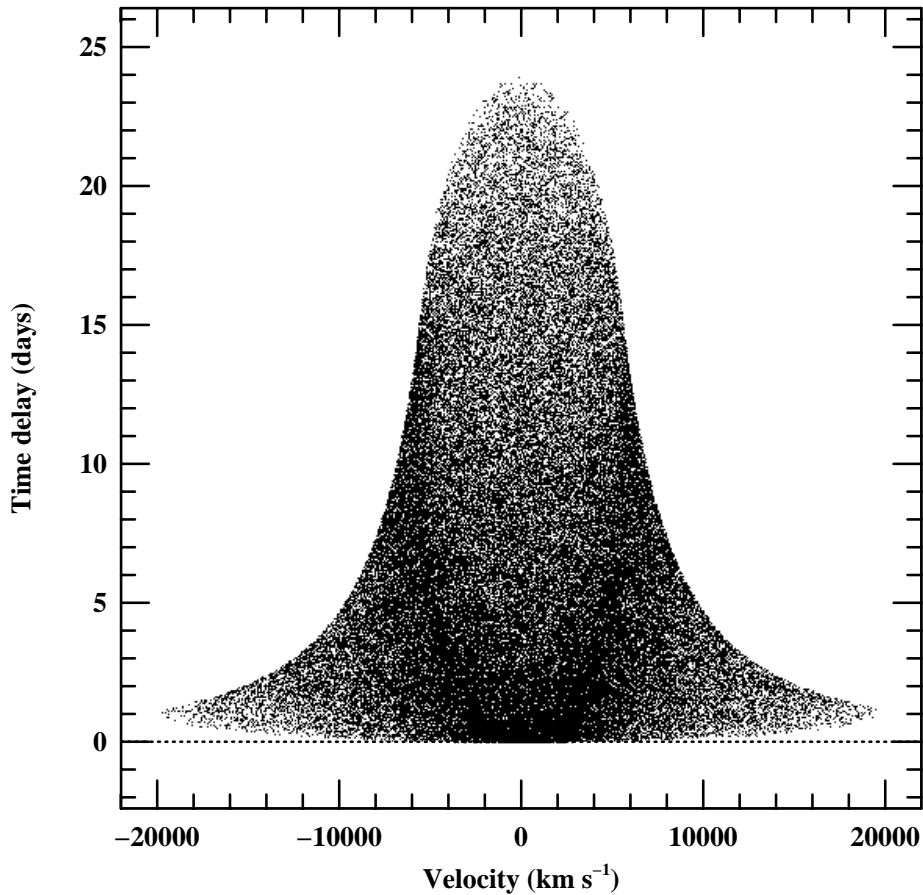


Figure 3. A model two-dimensional (i.e., response as a function of both line-of-sight velocity and time delay) transfer function. This model is consistent with the C IV $\lambda 1549$ response in NGC 5548 (Wanders et al. 1995), based on *HST* and *IUE* data from Korista et al. (1995).

have been specially adapted to these programs (see White & Peterson 1994 for a critical comparison of widely used methods, and Alexander’s paper in this volume for discussion of a new method).

As mentioned earlier, UV and optical spectroscopic monitoring of a few Seyfert galaxies during the 1980s constituted “proof-of-concept” for reverberation mapping; it was clear that the lines did indeed respond to continuum variations, on surprisingly short time scales (see Peterson 1988 for a summary of these early programs). The next step was to acquire suitable time series to measure the response time scales accurately, i.e., determine

the lags for various emission lines (eq. 5). As a practical matter, monitoring programs to achieve limited goals can be carried out at individual observatories. This has been demonstrated convincingly by ground-based results obtained at the Wise Observatory (e.g., Maoz et al. 1990, 1991; Netzer et al. 1990) at Ohio State University (e.g., Peterson et al. 1993; Kassebaum et al. 1997; Peterson et al. 1997), at CTIO (Winge et al. 1995, 1996), and at La Palma (by the “LAG” collaboration, whose work has been well summarized by Robinson 1994). However, probably the greatest success has been achieved by the large consortium known as the “International AGN Watch” (Alloin et al. 1994), which has carried out several multi-wavelength monitoring programs that have been anchored by UV spectroscopy with the *International Ultraviolet Explorer (IUE)* and the *Hubble Space Telescope (HST)* and optical spectroscopy with a large network of ground-based telescopes. The International AGN Watch efforts have included two major UV campaigns on NGC 5548 (Clavel et al. 1991; Korista et al. 1995) complemented by a continuing ground-based effort (Peterson et al. 1991, 1992, 1994; Dietrich et al. 1993; Romanishin et al. 1995), and similar campaigns on NGC 3783 (Reichert et al. 1994; Stirpe et al. 1994), Fairall 9 (Rodríguez-Pascual et al. 1997; Santos-Lleó et al. 1997), and 3C 390.3 (O’Brien et al. 1997; Dietrich et al. 1997). Other monitoring programs have been built around these projects, including extreme UV monitoring of NGC 5548 with the *Extreme Ultraviolet Explorer (EUVE)* (Marshall et al. 1997), a multi-wavelength snapshot of NGC 3783 (Alloin et al. 1995), and long-term X-ray monitoring of 3C 390.3 with *ROSAT* (Leighly et al. 1997). A purely ground-based campaign was also carried out on Mrk 509 (Carone et al. 1996). This group also undertook an intensive multi-wavelength program on NGC 4151 (Crenshaw et al. 1996; Kaspi et al. 1996a; Warwick et al. 1996; Edelson et al. 1996), although the limited duration of this experiment (about 10 days) precluded learning much about the emission-line response in this object.

The results on NGC 5548 (Korista et al. 1995) and NGC 4151 (Ulrich & Horne 1996) represent the state of the art in reverberation mapping. The transfer functions are not well-determined, as they are based on $\lesssim 50$ data points that are not noise-free. However, these two results are not likely to remain the last word on reverberation mapping for long: at the time of writing, the International AGN Watch is completing preliminary analysis of 49 days of nearly continuous observations of NGC 7469 with *IUE*, one of the high-priority “lasting value” projects undertaken during its nineteenth and final year of operations, which produced somewhat more than 200 independent spectra (Wanders et al. 1997). Intensive observations were made simultaneously with ground-based telescopes (Collier et al. 1997) and with the *Rossi X-Ray Timing Explorer (RXTE)* (Nandra et al. 1997).

Light curves for the UV continuum bands and emission lines are shown in Fig. 4, along with the cross-correlation functions.

4. Evaluation of Reverberation-Mapping Results

4.1. THE GAS DISTRIBUTION IN THE BLR

In this section, we attempt to answer the fundamental questions of reverberation mapping by evaluating the results of the more successful International AGN Watch campaigns. We address, in more detail, several of the uncertainties, and proceed to evaluate the significance of the available lag determinations. We then discuss the gas distribution in the BLR, as obtained by direct and indirect (inversion) methods.

4.1.1. *Limitations*

Obtaining well-sampled line and continuum light curves that are relatively noise free is only the first step towards the goal of a complete mapping of the gas distribution in the BLR. The interpretation of the data is not straightforward and there are various ambiguities and uncertainties. Three of the more critical problems are explained below.

1. A very severe limitation is the non-linear response of many emission lines. All lines are produced in a restricted zone inside the cloud and the line emissivity is a sensitive function of the incident ionizing flux, i.e., of the ionization parameter

$$U = \frac{Q}{4\pi R^2 n_{\text{H}} c}, \quad (7)$$

where Q is the rate at which the source produces ionizing photons (i.e., photons per second). Consider as an example C IV $\lambda 1549$, whose emission reflects both the size of the C⁺³ zone and the gas temperature over this region. This line flux increases linearly with the continuum flux only if most carbon is C⁺² or C⁺³. Further increase in the continuum level makes C⁺⁴ the dominant species and results in a large decrease in the emissivity of the line. The transfer function of C IV $\lambda 1549$ reflects the non-linear nature of the ionization process and the corresponding change in temperature. Most metal lines behave in a similar way, but over a different ionization-parameter range. The only exception is Ly α , whose response is close to linear under most conditions, since the line intensity directly reflects the number of ionizing photons absorbed by the gas. The Ly α line reacts non-linearly to the incident ionizing flux in two extreme cases; in low column-density clouds, the increased continuum level can make the gas fully transparent, thus reducing the

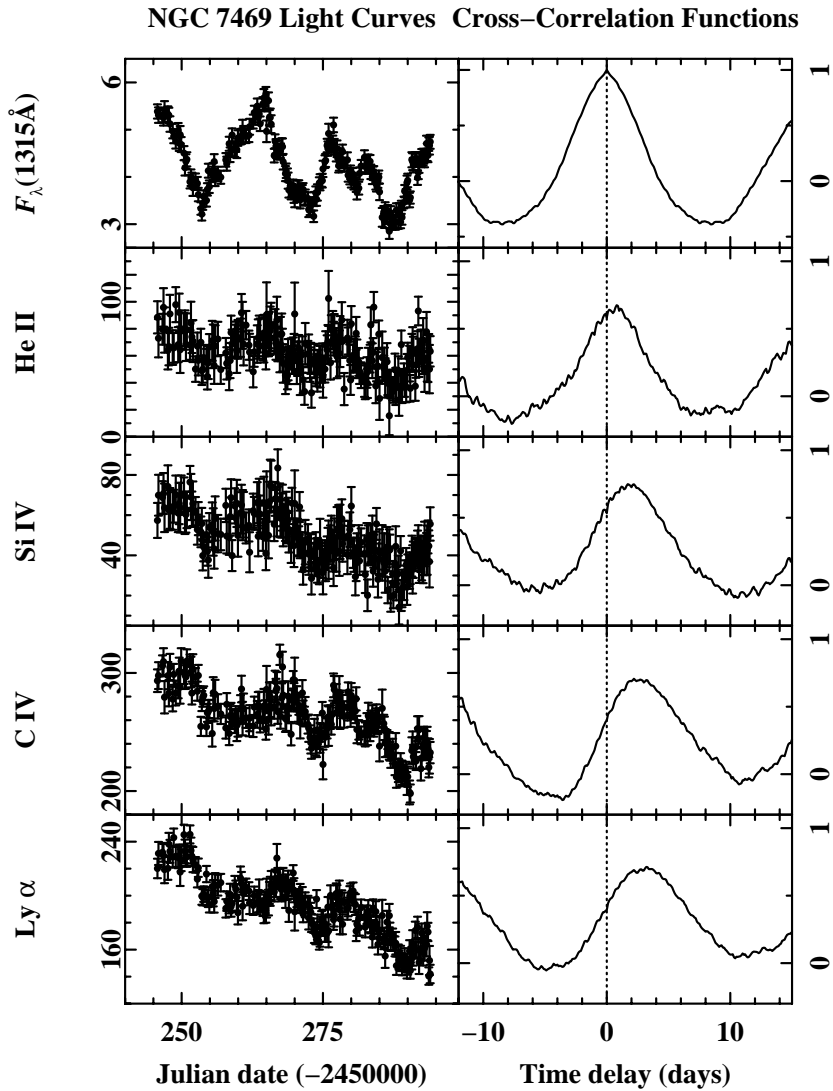


Figure 4. The left-hand columns show the light curves of NGC 7469 obtained with *IUE* during an intensive AGN Watch monitoring campaign during the summer of 1996. The right-hand column shows the result of cross-correlating the light curve immediately to the left with the 1315\AA light curve at the top of the left column; the panel at the top of the right column thus shows the 1315\AA continuum autocorrelation function. Data from Wanders et al. (1997).

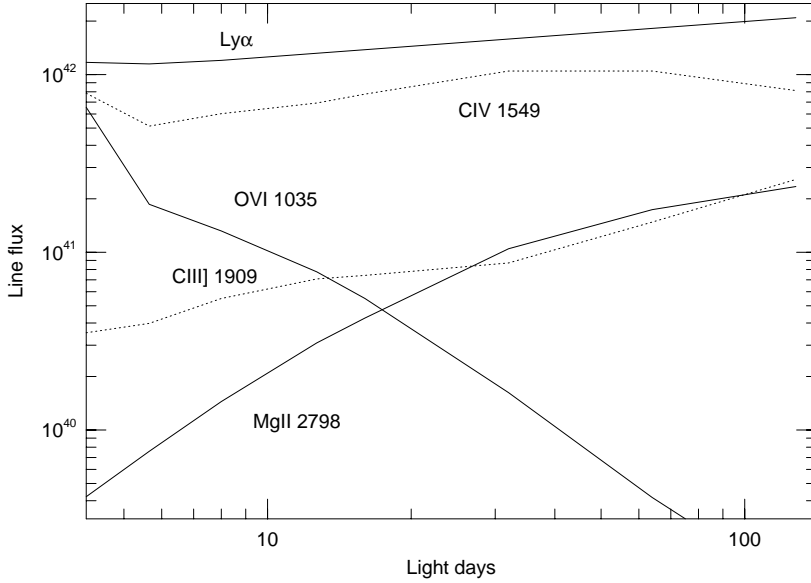


Figure 5. Line luminosity, per unit solid angle, as a function of distance from the center of NGC 5548 for an assumed gas distribution of $n_{\text{H}} \propto R^{-1}$ and $N_{\text{col}} \propto R^{-2/3}$.

line production considerably. In high column-density clouds, continuum variation can cause a significant change in the line optical depth $\tau(\text{Ly}\alpha)$ which will reduce the line emissivity due to line trapping and collisional suppression. Thus, non-linear effects are of great significance and affect the shape of the transfer function. Figure 5 illustrates the result of a particular set of photoionization calculations applied to the case of NGC 5548, the best observed Seyfert 1 galaxy. The model assumes a specific gas distribution given by $n_{\text{H}} \propto R^{-1}$, which results in a radial dependence of the ionization parameter, $U \propto R^{-1}$. The column density is obtained by assuming spherical clouds that retain their identity as they move in or out at their virial speed (for more details see Netzer 1990). The continuum luminosity is scaled to the luminosity of NGC 5548 during the 1989 campaign. With the measured $\text{Ly}\alpha$ lag of about 9 days, and the required, radius-averaged ionization parameter obtained from observed line ratios, this leaves little freedom for the choice of density at R_{in} . The diagram illustrates the constancy of some lines ($\text{Ly}\alpha$ and $\text{C IV } \lambda 1549$) and the dependence of other lines on the radius and ionization parameter ($\text{O VI } \lambda 1035$ and $\text{Mg II } \lambda 2798$) and the density ($\text{C III] } \lambda 1909$).

2. A second major source of uncertainty is the unknown shape and variability amplitude of the ionizing continuum. Multi-wavelength spectroscopy suggests that the shape of the optical–UV continuum changes with luminosity. It is thus reasonable to assume that the Lyman continuum, which drives the line luminosity, is changing its shape too. Present techniques assume that the variability of the ionizing flux is similar to the observed variability at much longer wavelengths, thus introducing an uncertainty into the transfer function. In principle, the shape of the ionizing continuum can be deduced from various line ratios; in practice, this is a difficult task.
3. Line emission from the BLR is not necessarily isotropic. The most notable example is $\text{Ly}\alpha$, whose emission pattern is likely to be beamed towards the central source because of the large column of neutral gas at the back of BLR clouds. A known beaming pattern can, in principle, be taken into account when calculating the transfer function (see Ferland et al. 1992), but present photoionization models cannot reliably calculate this pattern.

4.1.2. *Lag determination*

Even the simplest of all reverberation-mapping aims, the lag determination, is not a simple task since, in many cases, the line-to-continuum lag is only a small fraction of the typical variability time scale. Medium-luminosity Seyfert 1s are characterized by variability time scales of 30–100 days and lags of 2–6 days for the high-ionization lines. Since the lag is determined from the peak (or the center of gravity) of the CCF, which is the convolution of the ACF with the transfer function (eq. 5), the required accuracy is a small fraction of the CCF width. As noted earlier, there are several methods of determining the CCF, but none with a rigorous way of estimating the associated uncertainty. Thus, a slight misjudgment of the center of the asymmetric CCF gives a large uncertainty on the lag.

A simple, yet powerful method to determine the uncertainty associated with the lag is via Monte-Carlo simulations. This is done by guessing a plausible BLR model, computing its response to a given input signal, and then sampling the input and response light curves in a fashion similar to what was achieved in the actual experiment, including the effects of random and, in some cases, systematic errors. The assumed known parameters are the overall gas distribution (or, more precisely, the emissivity distribution of a particular line) and the driving continuum light curve. The observed continuum light curve is interpolated, in a predetermined way, to obtain the “known” continuum behavior. This smooth light curve is then fed through a pre-determined geometry, e.g., a thick shell with known R_{in} and R_{out} and emissivity as a function of radius, to obtain a predicted “line

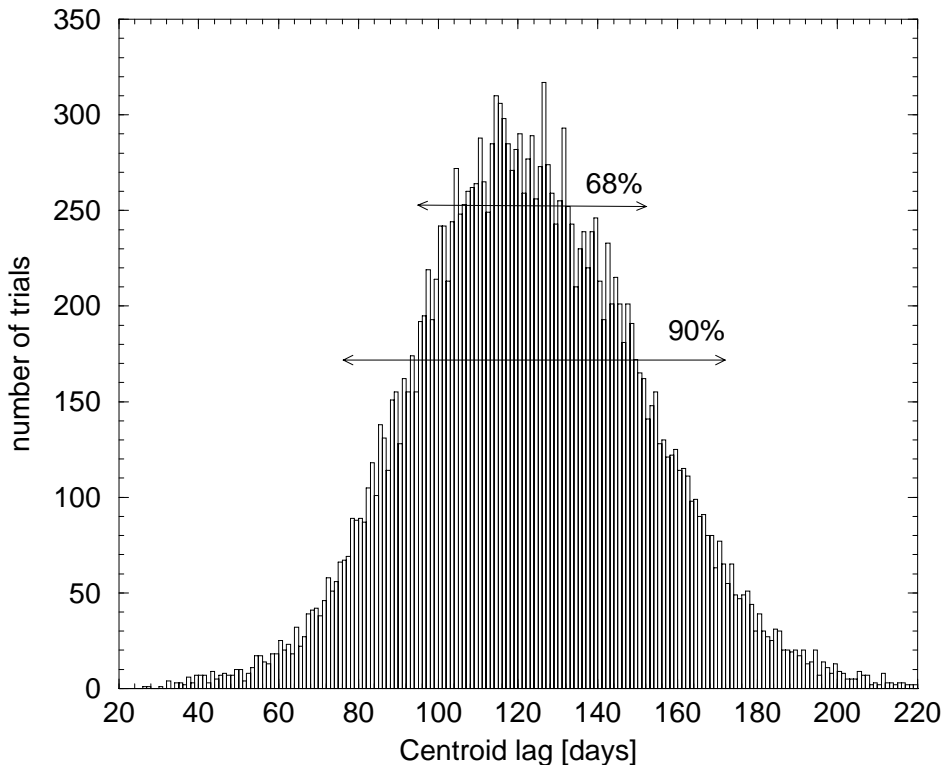


Figure 6. The CCPD histogram for the quasar PG 0804+762 (for the light curve see Kaspi et al. 1996b) assuming a thick spherical shell, extending from 20 to 200 light days, with line emission proportional to dR . The 68% and 90% intervals deduced from the simulations are shown.

light curve”. This line light curve is sampled in a pattern similar to the actual observations. A noise model is added to the “observations”, and the cross-correlation is performed, just as if these were real data, to obtain a CCF and its peak or centroid location. Many repetitions of this process produce a cross-correlation peak distribution (CCPD; Maoz & Netzer 1989) which gives, for the chosen geometry and observing pattern, the probability of finding the peak of the CCF inside a certain interval, say 3–5 days. This is probably the best way of assessing the reality of a particular lag determination and its associated uncertainty, for a given geometry. Figure 6 shows a specific example for a geometrically thick BLR in a luminous ($L = 2 \times 10^{45}$ ergs s^{-1}) quasar. The principal weakness of this method is that the results are only valid to the extent that the model is a reasonable representation of reality. Monte-Carlo methods require a complete set of pre-determined assumptions and are very useful in those cases where

the number of assumptions is small and the line response to continuum variability can be reliably simulated.

4.1.3. *Gas distribution using inversion methods*

Attempts to recover the one-dimensional transfer function (eq. 4) have been made for several sources, including NGC 4151 (Maoz et al. 1991), NGC 5548 (Horne, Welsh, & Peterson 1991; Krolik et al. 1991; Peterson et al. 1994; Wanders & Peterson 1996), Mrk 590 (Peterson et al. 1993), NGC 3516 (Wanders & Horne 1994), and NGC 3227 (Winge et al. 1995). In general, the data are insufficient to show any clear structure in $\Psi(\tau)$, although in many cases there is some evidence for very weak line response at $\tau \approx 0$, i.e., due to material along our line of sight to the continuum source. It has been suggested (Ferland et al. 1992; O’Brien, Goad, & Gondhalekar 1994) that this might be due to emission-line anisotropy, as explained earlier. There are still doubts, however, about whether or not the lack of line response at zero lag is in fact real (see Maoz 1997).

MEM methods are somewhat limited and, as shown by Horne (1994), can produce several different-looking transfer functions that fit the data equally well. The uncertainty in the width of such transfer function is large, due to the broad intrinsic ACF. In some cases the differences between acceptable solutions are large enough to prevent us from reaching even the simplest conclusions regarding the response at zero lag. The requirements on the amount and quality of the light-curve data are sufficiently demanding that we doubt that anyone would claim that today a unique and unambiguous solution has been found using inversion methods.

In only two cases have attempts been made at full recovery of $\Psi(v, \tau)$, in both cases for the C IV $\lambda 1549$ emission line, (1) using *HST* spectra of NGC 5548 (Wanders et al. 1995; Done & Krolik 1996), and (2) using *IUE* spectra of NGC 4151 (Ulrich & Horne 1996; see also Horne’s paper in this volume). In both cases, predominantly radial gas motions seem to be ruled out by the similarity of the response of the redshifted and blueshifted sides of the emission line. However, in both cases, there is quite a bit of ambiguity about the results, and the transfer-function structure is actually poorly determined. In the case of NGC 5548, the structure seems broadly consistent with the model shown in Fig. 3, as mentioned above (see Wanders et al. 1995). However, the details are not matched well by the model. Indeed there is a possible indication of an infalling component (Done & Krolik 1996) based on more rapid response of the red side of the line profile compared to the blue side, but which Wanders et al. (1995) dismiss as probably stochastic (i.e., the apparent “direction of flow” varies with time). Ulrich & Horne (1996) also suggest that there is a weak infall component present in the NGC 4151 data, but again, the signature is not unambiguous.

4.1.4. Gas distribution using direct (forward) methods

Inversion methods are designed to produce emissivity maps for specific lines while the physical picture we are after involves the run of density, column density, and cloud properties across the BLR. Unfortunately, there are large uncertainties in converting from emissivity maps to the desired physical maps, all associated with our limited understanding of the line production mechanism. The result is that, so far, there is not a single published model that can explain the light curves of all observed emission lines even in the best-studied AGN. It is therefore important to search for a simpler way of obtaining reliable information on some of the important parameters. This is provided by direct methods.

Direct methods make assumptions about the gas distribution and other properties and calculate, under these assumptions, the line intensity at every point and for every continuum flux level. The integrated line fluxes, as a function of time, are then compared with the observations. The procedure is easily followed in the particular case where all important properties, such as the gas density and column density, are given by smooth simple functions of the distance from the center (Netzer 1990). In such cases, the dependence of line emissivity on distance can be calculated by photoionization models and the procedure repeated a number of times with various assumed geometries. Final decision on the best chosen dependence is based on the model which best reproduces all of the emission lines.

Figure 7 illustrates two results of direct calculations applied to the Ly α light curve in the specific case of NGC 5548 discussed earlier (Fig. 5). In this case, all parameters are fixed by the assumed run of n_{H} with distance and the only missing assumptions are the values of R_{in} and R_{out} . The diagram compares the observed light curve with the model predictions for $R_{\text{in}}=4$ light days and two choices of R_{out} , 30 light days and 100 light days. For both of these we note the predicted lag and the quality of the fit (χ^2). Note that the assumed observational uncertainties are artificially increased, beyond those observed, for earlier times, to allow for the large uncertainty in the beginning of the campaign (see §2.1). Thus, at day 1, they are three times larger than the actual observed uncertainties (8% in this case). The diagram illustrates that the assumed density dependence is close, but not in perfect agreement with the observations. Better modeling requires somewhat different radial density dependence. The reality of such models should be assessed by checking the prediction for other emission-line light curves.

Diagrams like Fig. 7 suffer from the well-known non-linear response which is a problem in all lines, especially metal lines. There is, however, one measured quantity that is almost independent of this, the *total line emission* (Netzer 1990). Simple energy conservations arguments suggest that the total intensity of all emission lines equals the ionizing energy absorbed by

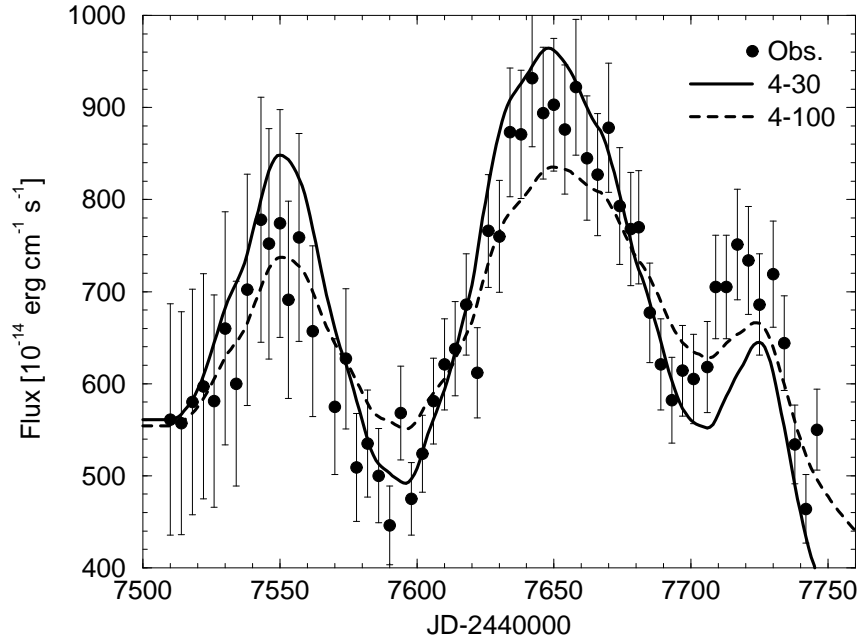


Figure 7. The observed Ly α light curve, from the 1989 NGC 5548 campaign, is compared with two predicted geometries involving $n_{\text{H}} \propto R^{-1}$. In both cases $R_{\text{in}} = 4$ light days and two different values of R_{out} , 30 and 100 light days. The value of χ^2 for 55 degrees of freedom is 75 for the small geometry and 54 for the large geometry. This χ^2 has been calculated with the shown error bars that have been artificially increased, for days 1–80, to allow for the unknown continuum behavior before the beginning of the campaign.

the cloud. Summing up the line intensities gives the almost-perfect and easiest-to-model light curve. This is “almost perfect” since the above sum involves some lines that are outside the observable range and some emission (mostly bound–free) that is difficult to measure. However, it is superior to all other methods and enables us, with some simple assumptions, to obtain a reliable estimate on the gas distribution. Robust direct methods are those that screen, out of all possible geometries, only those that are consistent with the “total line emission” light curve. The only major unknown in this procedure is the one associated with anisotropic line emission.

4.2. THE “NEW” BLR

Ten years of monitoring campaigns have resulted in a clearer view of AGN physics and in better understanding of the BLR. Inversion methods have provided some insight into the gas distribution and dynamics, but fall short

of resolving the more fundamental issues. Direct methods and lag determinations have resulted in some very meaningful new results and we feel it is time to compare the state of the field today to what it was ten years ago:

1. The size of the “old” BLR was determined indirectly from the best-estimated ionization parameter by making assumptions about the incident ionizing flux and the gas density. The 1997 BLR size is directly measured and is much smaller, by almost an order of magnitude.
2. The 1987 BLR was assumed to be “thin”, with $R_{\text{in}} \approx R_{\text{out}}$. The 1997 BLR is very thick, with $R_{\text{in}}/R_{\text{out}} \leq 0.1$. This is clearly demonstrated by the variable measured lags, in a single source, as a function of the continuum event duration (Netzer & Maoz 1990). It is verified by the shape of the derived transfer functions and by direct modeling.
3. When many lines have been observed in a single source, there is clear evidence for radial ionization stratification of the BLR, as the highest-ionization lines respond more rapidly than the lower-ionization lines. In NGC 5548, for example, N v $\lambda 1240$ and He II $\lambda 1640$ show lags of 1–2 days, Ly α and C IV have lags of 7–12 days, and H β responds even more slowly.
4. There is *some* evidence that the lag changes with time, at least in NGC 5548 (Peterson et al. 1994); H β lags ranging from 7 days (Netzer et al. 1990) to 22 days (Peterson et al. 1994) have been reported for this source, and indeed, the quantity we call the lag can vary on surprisingly short time scales.
5. The gross similarity of AGN spectra over a wide range in luminosity led, more than ten years ago, to a naïve prediction that the ionization parameter is almost independent of luminosity and thus $R_{\text{BLR}} \propto L^{1/2}$. Today we are seeing the first proof of this theoretical prediction through direct measurements of R_{BLR} in high-luminosity sources.

4.3. BLACK-HOLE MASS AND THE NATURE OF THE POWERHOUSE

Determining the black-hole mass was the most important motivation for all of the various AGN Watch monitoring campaigns. Such a determination must assume some kind of virial motion that is experimentally not yet proven. A key issue is the best combination of the BLR size and the gas velocity. The CCF peak, or the transfer function, provides an emissivity-weighted radius and, without a full dynamical model, it is not simple to choose the corresponding velocity. So far, the full-width at half maximum (FWHM) has been used in combination with this peak, but there are reasons to prefer the minimum inferred size R_{in} combined with the maximum observed velocity as obtained from the emission-line FWZI. Sharply peaked transfer functions, like those obtained for high-excitation lines, give the best

estimate for R_{in} . The uncertainty associated with the mass determination, due to the ambiguous size–velocity combination, is around a factor of two. Needless to say, the relative mass of different objects must be based on the same size determination, i.e., the transfer function or the CCF peak as determined for the same emission lines.

It is only recently that serious attempts to probe the nature of the powerhouse itself have been made. The common wisdom is that the AGN continuum is produced in close proximity to the central black hole, in a thin or slim disk. The X-ray continuum is produced in the innermost part of this structure while the optical-UV radiation is produced farther out. The two main ideas about the UV radiation involve the release of gravitational energy in the disk or the reprocessing of the central X-ray radiation (which, in itself, must be driven by accretion). A main problem is the energy budget since it is not obvious that the available X-ray energy can provide the energy observed in the UV flares.

Interestingly, the above two possibilities are associated with very different time scales. The viscous time determines the disk reaction to a change in accretion rate while the light-travel time gives the typical scale associated with X-ray reprocessing. Measuring the lag (if any) between X-ray and UV events could solve this issue. Using the standard thin disk assumptions we note that for such systems

$$T_{\text{eff}}^4 = \frac{3GM\dot{M}}{8\pi\sigma R^3} \left[1 - \left(\frac{R}{R_{\text{ms}}} \right)^{-1/2} \right], \quad (8)$$

where R_{ms} is the radius of marginal stability ($6R_g$ for Schwarzschild black hole and $1.22R_g$ for a maximally rotating Kerr hole) and we have neglected relativistic corrections. Assuming for simplicity that the frequency of the peak blackbody emissivity, $h\nu_{\text{max}} = 2.8kT$, represents the emission at every frequency, and adopting the simple $R \propto T^{-4/3}$ dependence, we get $R \propto \nu_{\text{max}}^{-4/3}$, or, using $r = R/R_g$,

$$r \approx 1.8 \times 10^{22} \nu_{\text{max}}^{-4/3} M_8^{-2/3} \dot{M}_{\odot}^{1/3}, \quad (9)$$

where $M_8 = M/10^8 M_{\odot}$ and \dot{M}_{\odot} is the accretion rate in solar masses per year. This couples the size and the location corresponding to a given maximum frequency of a given luminosity AGN. For example, the best values obtained for NGC 5548 ($M_8 \approx 0.5$, $\dot{M}_{\odot} \approx 0.07$) combined with a Schwarzschild black hole, gives a separation between the optical (5000 Å) and the UV (1400 Å) peak emission locations that corresponds to about 0.6 light days. This spacing suggests a short light-travel time and a very long viscous time for the correlated UV and optical continuum variability

in this source. The light-travel time is consistent with the measured upper limit (less than two days; see Korista et al. 1995).

Prior to the recent NGC 7469 campaign, there was no real measurement of optical–UV or UV–X-ray continuum lags. This is likely to change soon and the results will definitely shed new light on this issue and may enable us, for the very first time, to distinguish between the simple disk model and the reprocessing idea.

4.4. LUMINOSITY–SIZE–MASS RELATIONSHIP FOR AGN

One of the exciting results reported in this meeting is the first meaningful size–luminosity relationship for AGN (Kaspi et al. 1996b, and Kaspi’s contribution to these proceedings). For the first time, we have a large enough AGN sample covering almost two orders of magnitude in luminosity and showing a clear trend of H β lag as a function of luminosity. The best-fitted lag–luminosity slope is very close to the predicted $R \propto L^{1/2}$ relationship, and the resulting size is approximately

$$R_{\text{BLR}} = 0.014L_{44}^{1/2} \text{ pc} \quad (10)$$

where L_{44} is the 0.1–1 μm luminosity in units of $10^{44} \text{ ergs s}^{-1}$ (we have assumed $H_0 = 75 \text{ km s}^{-1} \text{ Mpc}^{-1}$ and $q_0 = 0.5$).

The search for an L – M relationship involves yet another correlation of L with the emission-line FWHM. Unfortunately, the sample used for determining the L –size correlation is too small and the spread in line width too weak to use it for this purpose. Reports in the literature involving much larger samples suggest anything from FWHM independent of L to $\text{FWHM} \propto L^{1/4}$. Obviously, strong selection effects that are not well understood are involved. It is also becoming apparent that the broad-line widths depend on X-ray properties (Boller et al. 1996) and that different lines can show different widths and dependences. Given all this, and the experimentally verified $R_{\text{BLR}} \propto L^{1/2}$, it is probably safe to say that the black-hole mass determination is consistent with anything from $M \propto L$ to $M \propto L^{1/2}$, with a factor 2–4 uncertainty on the normalization of this relationship.

5. Future Reverberation-Mapping Experiments

The last 10 years were so full of surprises that we shall not risk predicting the 10 coming ones. Instead, we comment on what can be done, and should be tried, with present-day capabilities.

5.1. IMPROVED SAMPLING AND MULTI-WAVELENGTH CAMPAIGNS

Improved sampling has already resulted in some spectacular results. The recent dense sampling of NGC 4151 (Crenshaw et al. 1996, Kaspi et al. 1996a) has shown continuum variability on extremely short time scales, and the soon-to-be-published results of the NGC 7469 monitoring (Fig. 4) will no doubt raise some new questions about the origin of the UV and X-ray continuum.

Unfortunately, there is not much hope for repeating the long-duration (many months), dense-sampling campaigns like those that involved the late *IUE*. *HST* observations can provide superior data that are extremely important for continuum measurements but of insufficient duration for dense sampling of emission lines. Some X-ray satellites, like *RXTE*, are suitable for dense, high-frequency sampling, but it seems unlikely that *AXAF* or *XMM* will spend such long times on individual targets.

Multi-wavelength campaigns are likely to continue to be the most important way of probing the physics of the BLR, with important implications for the continuum-emitting source. The combination of X-ray information with data at lower photon energies is crucial. While ground-based telescopes are likely to contribute a lot in this area, the weak link is the UV, which now depends almost solely on *HST*. Long-term *HST* programs are definitely necessary to proceed in this direction.

It is important to note that *SRG* (to be launched at the end of 1998) will carry on board two X-ray telescopes (*SODART* and *JET-X*) and a UV telescope (*TAUVEX*) that are capable of producing the required long-term multi-wavelength continuum monitoring. No coordination is required in this case since all telescopes on board this mission are looking at the same field. It remains to be seen whether the observing program of the satellite will allow the very long observations required for such projects.

5.2. LARGE-AREA, MULTI-OBJECT CAMPAIGNS

Most AGN campaigns, so far, have concentrated on detailed studies of individual objects. The result is a small sample covering a limited range in luminosity and redshift. Very high-luminosity, high- z quasars are completely missing.

Future campaigns will be able to use multi-aperture fiber-fed spectrographs to improve on this situation. Such a technique will allow repetitive observations of several dozens of AGN, in the same field, for a long period of time. Infrequent visits, e.g., every couple of weeks, are definitely adequate to secure a large sample of high- z quasars and to measure their BLR sizes. Given the predicted values of R_{BLR} and the high redshifts, such a campaign would probably require 5 to 10 years.

5.3. FUTURE ROLE OF THE WISE OBSERVATORY AND OTHER SMALL TELESCOPES

While future spectroscopy of large, high- z AGN samples is limited to large telescopes, small telescopes are still very important. They can provide frequent, broad-band imaging of the same fields thus adding many more points to the continuum light curves. As shown in many previous campaigns, adequate sampling of the continuum light curve is a critical issue. Emission lines react slowly to continuum variations and their sampling, given a well-constrained continuum, is less crucial. Small telescopes with large fields of view, like the 1-m telescope at the Wise Observatory, can easily provide high-frequency continuum observations of luminous AGN to supplement the spectroscopic observations by the large telescopes.

BMP gratefully acknowledges support for reverberation-mapping studies at Ohio State University by the US National Science Foundation through grant AST-9420080 and by NASA through Long-Term Space Astrophysics Grant NAG5-3233 and Astrophysics Data Program Grant NAG5-3497. Monitoring of AGN at the Florence and George Wise Observatory is supported by the Israel Science Foundation and by the Raymond and Beverly Sackler Institute of Astronomy.

References

- Alloin, D., Clavel, J., Peterson, B. M., Reichert, G. A., & Stirpe, G. M. 1994, in *Frontiers of Space and Ground-Based Astronomy*, ed. W. Wamsteker, M. S. Longair, & Y. Kondo (Dordrecht: Kluwer), p. 423
- Alloin, D., et al. 1995, *A&A*, 293, 293
- Blandford, R. D., & McKee, C. F. 1982, *ApJ*, 255, 419
- Boller, Th., Brandt, W.N., & Fink, H. 1996, *A&A*, 305, 53
- Carone, T. E., et al. 1996, *ApJ*, 471, 737
- Clavel, J., et al. 1991, *ApJ*, 366, 64
- Collier, S., et al. 1997, in preparation
- Crenshaw, D. M., et al. 1996, *ApJ*, 470, 322
- Dietrich, M., et al. 1993, *ApJ*, 408, 416
- Dietrich, M., et al. 1997, in preparation
- Done, C., & Krolik, J. H. 1996, *ApJ*, 463, 144
- Edelson, R., et al. 1996, *ApJ*, 470, 364
- Ferland, G. J., Peterson, B. M., Horne, K., Welsh, W. F., & Nahar, S. N. 1992, *ApJ*, 387, 95
- Goad, M., & Wanders, I. 1996, *ApJ*, 469, 113
- Horne, K. 1994, in *Reverberation Mapping of the Broad-Line Region in Active Galactic Nuclei*, ed. P. M. Gondhalekar, K. Horne, & B. M. Peterson, ASP Conference Series Vol. 69 (San Francisco: ASP), p. 23
- Horne, K., Welsh, W. F., & Peterson, B.M. 1991, *ApJ*, 367, L5
- Kaspi, S., et al. 1996a, *ApJ*, 470, 336
- Kaspi, S., Smith, P. S., Maoz, D., Netzer, H., & Jannuzi, B. T. 1996b, *ApJ*, 471, L75
- Kaspeba, T. M., Peterson, B. M., Wanders, I., Pogge, R. W., Bertram, R., & Wagner, R. M. 1997, *ApJ*, 475, 106

- Korista, K. T., et al. 1995, ApJS, 97, 285
- Krolik, J. H., & Done, C. 1995, ApJ, 440, 166
- Krolik, J. H., Horne, K., Kallman, T. R., Malkan, M. A., Edelson, R. A., & Kriss, G. A. 1991, ApJ, 371, 541
- Leighly, K. M., O'Brien, P. T., Edelson, R., George, I. M., Malkan, M. A., Matsuoka, M., Mushotzky, R. F., & Peterson, B. M. 1997, ApJ, in press
- Maoz, D. 1997, in *Emission Lines in Active Galaxies: New Methods and Techniques*, ed. B. M. Peterson, F.-Z. Cheng, & A. S. Wilson, ASP Conference Series Vol. 113 (San Francisco: ASP), p. 138
- Maoz, D., & Netzer, H. 1989, MNRAS, 236, 21
- Maoz, D., Netzer, H., Leibowitz, E., Brosch, N., Laor, A., Mendelson, H., Beck, S., Almoznino, E., & Mazeh, T. 1991, ApJ, 367, 493
- Maoz, D., Netzer, H., Mazeh, T., Beck, S., Almoznino, E., Leibowitz, E., Brosch, N., Mendelson, H., & Laor, A. 1990, ApJ, 351, 75
- Marshall, H. L., Carone, T. E., Peterson, B. M., Clavel, J., Crenshaw, D. M., Korista, K. T., Kriss, G. A., Krolik, J. H., Malkan, M. A., Morris, S. L., O'Brien, P. T., & Reichert, G. A. 1997, ApJ, 479, 222
- Nandra, K., et al. 1997, in preparation
- Netzer, H. 1990, in *Active Galactic Nuclei*, R.D. Blandford, H. Netzer, and L. Woltjer (Berlin: Springer-Verlag), p. 57
- Netzer, H., & Maoz, D. 1990, ApJ, 365, L5
- Netzer, H., Maoz, D., Laor, A., Mendelson, H., Brosch, N., Leibowitz, E., Almoznino, E., Beck, S., & Mazeh, T. 1990, ApJ, 353, 108
- O'Brien, P. T., Goad, M. R., & Gondhalekar, P. M. 1994, MNRAS, 268, 485
- O'Brien, P. T., et al. 1997, in preparation
- Penston, M. V. 1991, in *Variability of Active Galactic Nuclei*, ed. H.R. Miller & P.J. Wiita (Cambridge, Cambridge Univ. Press), p. 343
- Pérez, E., Robinson, A., & de la Fuente, L. 1992, MNRAS, 256, 103
- Peterson, B. M. 1988, PASP, 100, 18
- Peterson, B. M. 1993, PASP, 105, 247
- Peterson, B. M., et al. 1991, ApJ, 368, 119
- Peterson, B. M., et al. 1992, ApJ, 392, 470
- Peterson, B. M., et al. 1993, ApJ, 402, 469
- Peterson, B. M., et al. 1994, ApJ, 425, 622
- Peterson, B. M., et al. 1997, in preparation
- Pijpers, F. P., & Wanders, I. 1994, MNRAS, 271, 183
- Reichert, G. A., et al. 1994, ApJ, 425, 582
- Robinson, A. 1994, in *Reverberation Mapping of the Broad-Line Region in Active Galactic Nuclei*, ed. P. M. Gondhalekar, K. Horne, & B. M. Peterson, ASP Conference Series Vol. 69 (San Francisco: ASP), p. 147
- Rodríguez-Pascual, P. M., et al. 1997, ApJS, in press
- Romanishin, W., et al. 1995, ApJ, 455, 516
- Santos-Lleó, M., et al. 1997, ApJS, in press
- Stirpe, G. M., et al. 1994, ApJ, 425, 609
- Ulrich, M.-H., & Horne, K. 1996, MNRAS, 283, 748
- Wanders, I., et al. 1995, ApJ, 453, L87
- Wanders, I., & Horne, K. 1994, A&A, 289, 76
- Wanders, I., & Peterson, B. M. 1996, ApJ, 466, 174
- Wanders, I., et al. 1997, ApJS, in press
- Warwick, R., et al. 1996, ApJ, 470, 349
- Welsh, W. F., & Horne, K. 1991, ApJ, 379, 586
- White, R. J., & Peterson, B. M. 1994, PASP, 106, 879
- Winge, C., Peterson, B. M., Horne, K., Pogge, R. W., Pastoriza, M. G., Storchi-Bergmann, T. 1995, ApJ, 445, 680
- Winge, C., Peterson, B. M., Pastoriza, M. G., Storchi-Bergmann, T. 1996, ApJ, 469, 648